IEEE Access
Multidisciplinary | Rapid Review | Open Access Journal

Received January 30, 2021, accepted February 19, 2021, date of publication February 24, 2021, date of current version April 5, 2021.

*Digital Object Identifier 10.1109/ACCESS.2021.3061970*

# Wideband SIW Half-Mode/Quarter-Mode-Fed Microstrip Patch Complementary Antennas With Back Radiation Suppression

**LIPING YUAN[1], KAI SUN[1], SIHAO LIU[2], BO CHEN[1], (Member, IEEE), AND DEQIANG YANG[1], (Member, IEEE)**

[1]School of Electronic Science and Engineering, University of Electronic Science and Technology of China (UESTC), Chengdu 611731, China
[2]School of Materials and Energy, University of Electronic Science and Technology of China (UESTC), Chengdu 611731, China

Corresponding author: Deqiang Yang (dqyang@uestc.edu.cn)

This work was supported by the Foundation for Innovative Research Group of the National Natural Science Foundation of China under Grant 61721001.

**ABSTRACT** Complementary sources concept and half-mode/quarter-mode substrate integrated waveguide (HMSIW/QMSIW) technology are introduced in this paper to improve the back-radiation suppression and bandwidth of microstrip patch antennas (MPAs). The HMSIW cavity as the feeding structure brings an additional resonant frequency to the inherent resonant mode of typical MPAs, which efficiently extends the bandwidth of the MPAs. In addition, while stimulating the MPA mode, the HMSIW cavity drives a monopole by slightly breaking the shorting wall of the HMSIW cavity and loading a printed monopole. The loaded monopole and the equivalent magnetic currents of the MPA construct an orthogonal complementary source model that indicates back radiation suppression. A differential feeding scheme is also employed to enhance the radiation performance. The dual-polarized model, achieved by replacing the HMSIW cavity with QMSIW cavities, is also addressed and even fabricated and tested. The measured results show a differential impedance bandwidth of 15.4% from 1.91 GHz to 2.23 GHz with a differential port-to-port isolation of 38 dB. In the operating band, the average gain is 7.5 dBi, and the front-to-back ratio (FBR) is over 18 dB with a maximum value of 34 dB.

**INDEX TERMS** Half-mode, quarter-mode, complementary sources, front-to-back ratio, microstrip patch antenna.

## I. INTRODUCTION

DUE to their attractive properties, including low cost, light weight, and ease of integration, microstrip patch antennas (MPAs) have been widely adopted in many modern communication systems [1]. Because of this, MPAs have been thoroughly studied and developed since the 1950s. Traditional MPAs always suffer from narrow bandwidths [2], [3]. Since the bandwidth can be improved by increasing the thickness of the substrate, this is not a qualitative change.

In recent decades, much new researches have been devoted to expanding the bandwidth of microstrip patch antennas, for example, by introducing parasitic elements [4]–[7], improving feeding schemes (L-shaped probes [8], [9], using meandering probes [10], [11], applying slot coupling feeding [12], [13]) and reallocating several radiative modes [14]–[17]. All of these techniques can enhance the bandwidth of MPAs to meet the bandwidth requirements of many communication systems but are accompanied by the deterioration of other types of antenna performance, such as high cross-polarization [8], [9], large side lobes [14]–[17] or strong back radiation [12], [13], [18].

Although these broadband technologies cause more or less performance degradation, almost all the types of degradation have related specialized research and literature related to overcoming them, including cross-polarization suppression [19], [20], side-lobe suppression [14], harmonic suppression [21]–[23] and so on. However, studies and analyses on back radiation suppression are relatively rare. The studies focusing on improving the front-to-back ratio (FBR) of MPAs always utilize metamaterial reflectors [24], [25], which usually require additional substrate layers or a large size. Indeed, as communication systems become increasingly compact, the aperture that can be supplied to the antenna decreases.

The associate editor coordinating the review of this manuscript and approving it for publication was Tutku Karacolak.

It is also increasingly unacceptable to utilize a sufficiently large ground plane to achieve a high FBR for MPAs. Implementing a broadband microstrip antenna in a compact space while suppressing the backward radiation of the antenna has become a problem worthy of attention.

In this paper, we introduce half-mode/quarter-mode substrate integrated waveguide (HMSIW/QMSIW) techniques [26], [27] to excite MPAs for enhanced bandwidth. Meanwhile, complementary sources technology [28], [29] is also adopted to improve the FBR performance. When the MPAs are stimulated, a loaded monopole is also fed by the improved HMSIW/QMSIW cavity, so orthogonal complementary sources are constructed to suppress the back radiation [30]–[32]. In addition, a differential feeding scheme is also adopted. On other hand, differential feeding scheme can ensure a symmetrical radiation pattern and low cross-polarization [14], [15], [33]. On the other hand, integrating differential antennas with differential circuits can achieve a higher integration and efficiency [34], [35]. A differential dual-polarized MPA, achieved by two pairs of orthogonal monopole-loaded QMSIW cavities, is fabricated and tested. The measured results show a bandwidth enhanced by 15.4% with a high differential port-to-port isolation of over 38 dB. Due to the introduction of complementary source technology, the maximum value of FBR is extended to 34 dB with an average gain of 7.5 dBi.

## II. PRINCIPLE OF OPERATION

### A. HMSIW/QMSIW CONCEPT

A typical rectangular SIW resonator under the dominant mode is shown in Fig. 1, and its resonant characteristics have been thoroughly analyzed in previous reports [26]. Due to the high ratio of width to height for the SIW resonator, the electric-field distribution is nearly uniform in the z-direction, so the magnetic field is always vertical to the symmetrical planes (AA', BB', CC', DD'), and these symmetric planes of the SIW are equivalent to magnetic walls.

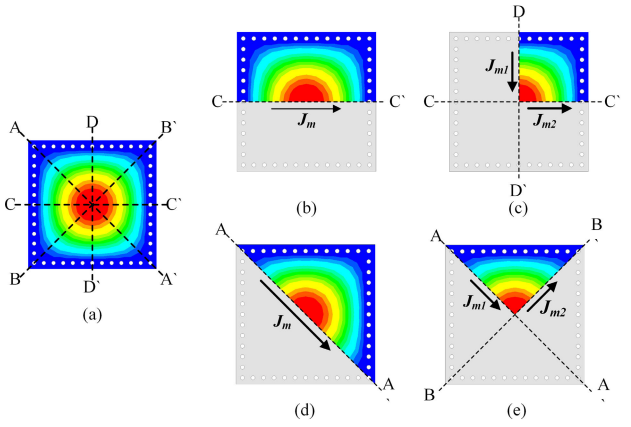


**FIGURE 1.** The E-field distribution diagram in the SIW cavity under (a) the original SIW mode, (b) half-mode by the horizontal axis, (c) quarter-mode by the horizontal and vertical axes, (d) half-mode by the diagonal and (e) quarter-mode by the diagonal.

Hence, when half of the metal cover along the symmetry plane (Fig. 1(b) and Fig. 1(d)), or even three quarters (Fig. 1(c) and Fig. 1(e)) is removed, the electromagnetic field distribution in the rest can remain approximately intact.

Although in the HMSIW/QMSIW cavity (Fig. 1(c) and Fig. 1(e)), the field distribution can still be kept roughly the same as that in the original SIW cavity (Fig. 1(a)), the electromagnetic energy is inevitably radiated in part from the open edges, and this characteristic is even used as a radiation source in antenna design in the millimeter wave (mmW) band [26], [27]. The radiation process can be equivalent to magnetic current radiation sources parallel to the open edge because the edge electric field in the HMSIW/QMSIW cavity is always vertical to the open edge. Hence, the magnetic field distribution is parallel to the open edges of the HMSIW/QMSIW cavity, which makes it possible to work as a magnetically excited source in MPAs.

### B. HMSIW-EXCITED MPA

The HMSIW/QMSIW cavities can work as antennas in the mmW band, while they are not efficient enough in the lower frequency band due to the ultralow profile. However, HMSIW cavities can be applied in magnetic-excited MPAs working as a feeding structure (Fig. 2) as an option that can be used instead of aperture-coupling feeding [12], [13] and torsion-coil coupling feeding [36]. Taking the HMSIW model shown in Fig. 1(b) as an example, the equivalent magnetic currents generated by the HMSIW cavity can also excite MPAs, as shown in Fig. 2(b)). Obviously, this feeding scheme can avoid a complicated 3D structure and even keep the ground plane integrated.

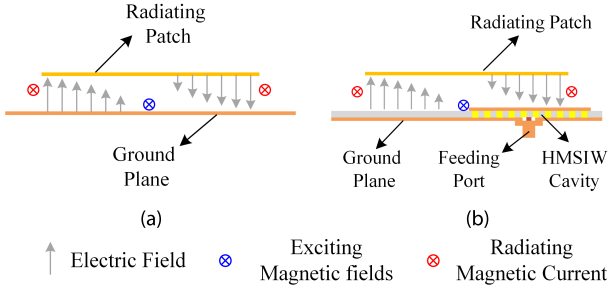


**FIGURE 2.** The magnetic-current-fed MPA model. (a) Typical magnetic-current-fed MPA model [12], [13], [36] and (b) HMSIW-fed MPA model.

The typical MPA has an inherent resonant mode, and introducing the HMSIW cavity as the feeding structure can introduce an additional resonance mode. The dual-mode resonance can efficiently expand the bandwidth compared to the original single-mode resonance of the typical MPA. The equivalent circuit of HMSIW-fed MPA is shown in Fig. 3(a), and dual-mode resonance feature of the two-order resonator (Fig. 3(b)) can be noticed and that is the basis of broadband performance. Obviously, the HMSIW cavity works only as the excitation of MPAs and can be regarded as a lossless resonator if ignoring the dielectric loss and metal loss, so the

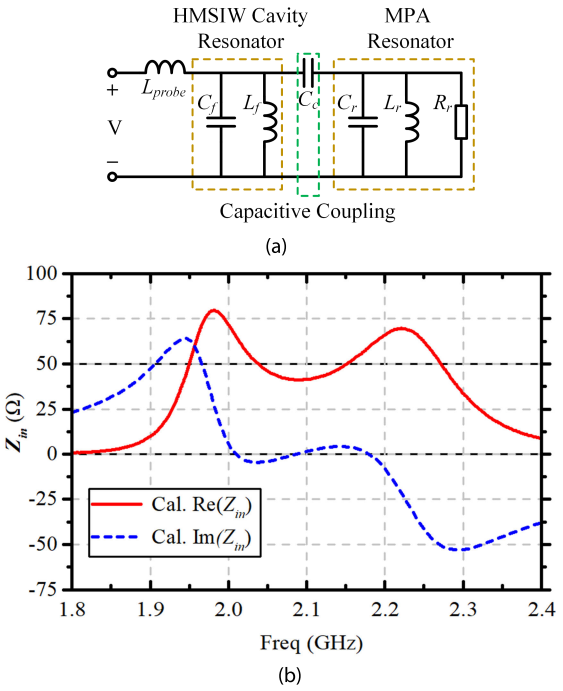


**FIGURE 3.** The equivalent model and frequency response characteristics of the HMSIW-fed MPA. (a) Equivalent circuit model and (b) calculated frequency response characteristics.

radiation mode throughout the wide band is a fixed MPA mode, which indicates a stable radiation performance, including a stable gain and radiation pattern.

### C. SIW-DRIVEN MONOPOLE

As shown in Fig. 2(b), the radiating magnetic currents are parallel to the edges of the radiation patch. Hence, to construct the complementary sources for back radiation suppression, it is necessary to construct an electric antenna that is placed perpendicular to the magnetic current element. Dipoles and monopoles are common electrical antenna options, especially bow-tie-shaped dipoles and triangular monopoles, which are always able to achieve excellent wide bandwidth performance.

Therefore, a new model, shown in Fig. 4(a), is considered, and several shorting vias of the SIW cavity are cancelled where a trapezoidal stub is loaded simultaneously. The minor damage does not substantially alter the characteristics of the SIW cavity, so it can maintain its dominant mode state. The junction can also maintain the voltage zero state (wave node), and the end of the monopole is the voltage antinode, so the loaded stub can work in a monopole state. The field distribution feature in HMSIW is similar to that of the original SIW cavity. The same operation can operate in the HMSIW cavity, and the monopole-integrated HMSIW model is shown in Fig. 4(b). Then, using the improved HMSIW cavity to replace the original HMSIW-fed MPAs (Fig. 4(c)), a complementary-source-based MPA is achieved. As shown in Fig. 5(a), the magnetic current is orthogonal to the electric

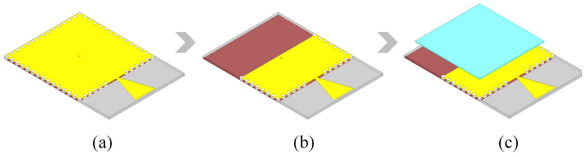


**FIGURE 4.** Evolution process of the complementary MPA. (a) SIW-fed monopole, (b) HMSIW-fed monopole and (c) complementary MPA.

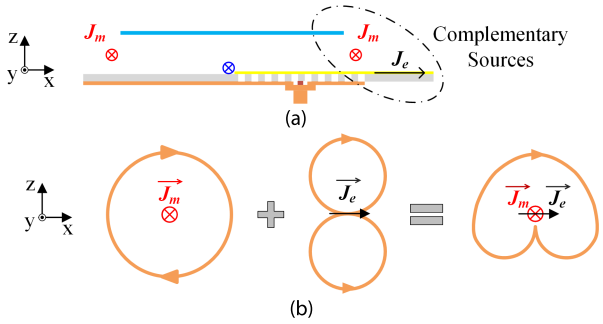


**FIGURE 5.** The diagram of the complementary MPA. (a) Radiation sources of the complementary MPA and (b) the back-radiation suppression mechanism of the complementary sources.

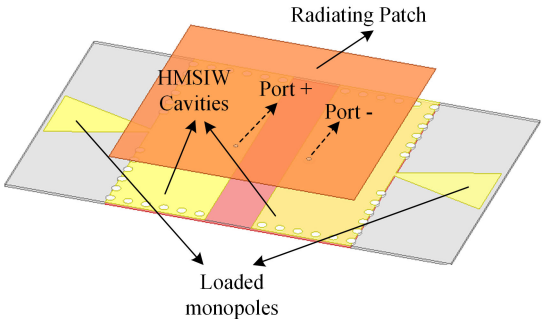


**FIGURE 6.** The configuration of the differential HMSIW-fed complementary MPA.

sources, so the foundation of enhanced back radiation suppression is available (Fig. 5(b)).

## III. ANTENNA ANALYSIS

### A. DIFFERENTIAL HMSIW-FED COMPLEMENTARY MPAs

Due to the inherent high pattern symmetry and low cross-polarization performance of the differential antenna, a differential feeding scheme is introduced in these HMSIW-fed MPAs for more obvious analysis of the back radiation suppression characteristics. The configuration of the differential HMSIW-fed complementary MPA is shown in Fig. 6. The radiation patch of the MPAs is the same size as the ground plane. Two differentially fed HMSIW cavities simultaneously drive the MPA and a pair of monopoles.

To better reveal the improvement from the differential HMSIW-fed complementary concept, two reference antennas (Ant. I and Ant. II) are introduced here for comparison with the proposed complementary MPA (Ant. III). As shown in Fig. 7(a), Ant. I is a typical MPA driven by a pair differential probe, and Ant. II is a conventional differential HMSIW-fed MPA without complementary sources. For a fair

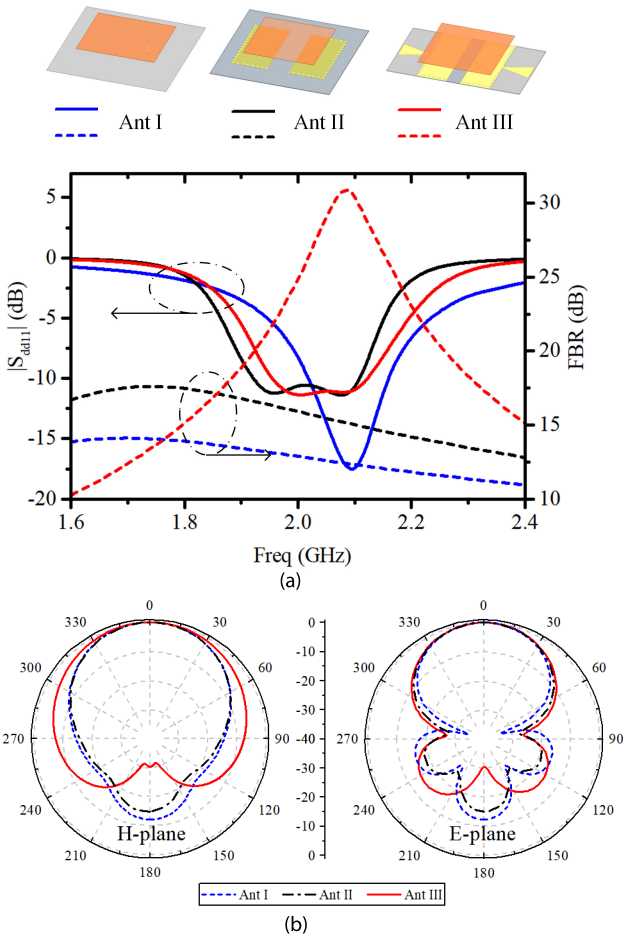


**FIGURE 7.** A port and radiation performance comparison of the different MPAs. (a) The $S_{11}$ and FBR curves and (b) normalized radiation patterns at 2.1 GHz.

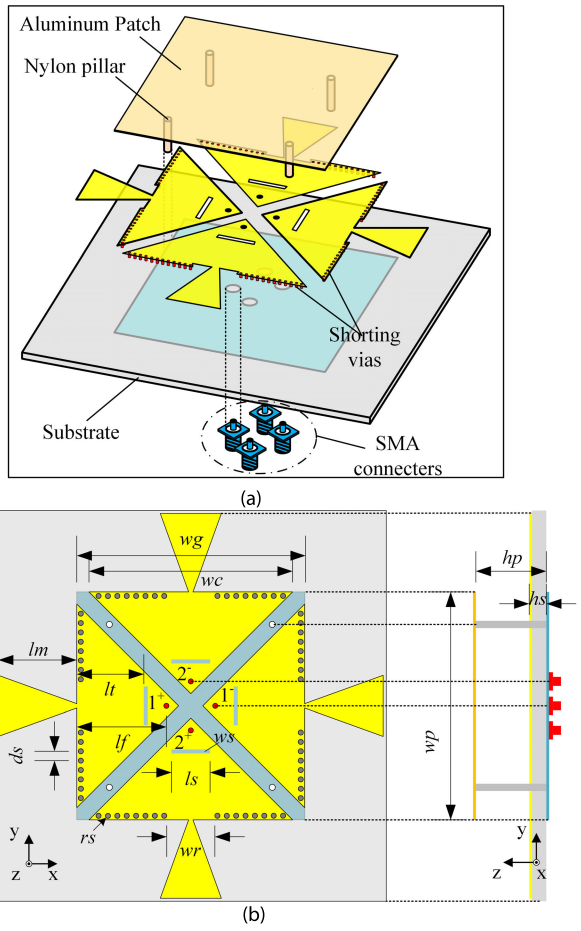


**FIGURE 8.** The configuration and detailed parameters of the differential QMSIW-fed dual-polarized complementary MPA. (a) 3D-view and (b) top-view and side-view. *wp* = 56 *mm*, *wc* = 50 *mm*, *wg* = 56 *mm*, *lf* = 22 *mm*, *wr* = 12 *mm*, *ls* = 10 *mm*, *ws* = 1 *mm*, *lm* = 19.4 *mm*, *wm* = 15 *mm*, *lt* = 16.2 *mm*, *ds* = 1.5 *mm*, *rs* = 0.3 *mm*.

comparison, the ground planes of both Ant. I and Ant. II are expanded to ensure that the three models have the same size.

As shown in Fig. 7(a), the differential-mode reflection coefficient $S_{dd11}$ and FBR curves are compared. The resonant characteristics change from single-mode resonance to dual-mode resonance when the model evolved from Ant. I to Ant. II, which indicates an enhanced impedance bandwidth. A comparison of Ant. II and Ant. III shows that the shrinking ground-plane size and the additional monopoles have no essential influence on the port performance. The introduced complementary sources concept substantially improves the FBR performance of the MPA. The maximum boost is at 2.1 GHz over 30 dB, which is a 16 dB improvement over that of Ant. II. The FBR curves of Ant. I and Ant. II exhibit similar trends but are worse overall than those of Ant. I. This occurs because to make the three models resonate at approximately the same frequency, the radiation patch of Ant. I is larger than those of the other two. From another perspective, as compared in Fig. pattern, the radiation patterns of two reference antennas (Ant. I and Ant. II) exhibit an obvious back lobe, while the proposed differential HMSIW-fed complementary MPA (Ant. III) exhibits obvious zero radiation in the back direction. This radiation pattern comparison also demonstrates the ability of the introduced complementary source technology to suppress the backward radiation of a compact microstrip antenna.

### B. DIFFERENTIAL QMSIW-FED DUAL-POLARIZED COMPLEMENTARY MPAs

Compared to an HMSIW resonant structure, the QMSIW resonant cavity has significant advantages and a more compact structure that make dual-polarized complementary MPAs possible. As shown in Fig. 8, two pairs of orthogonally placed differential QMSIW cavities excite the orthogonal $TM_{10}$ and $TM_{01}$ modes of MPAs. Naturally, every QMISW cavity is loaded with a monopole, and the whole structure is a rotationally symmetric structure, which conceals a theoretically infinite differential port-to-port isolation. Note that the HMSIW cavity is designed by selecting coordinate axis segmentation (Fig. 1(b)), while the QMSIW cavity is based on diagonal segmentation (Fig. 1(e)), which can be attributed to a complete shorting edge of the SIW cavity and facilitates the integration of monopoles.

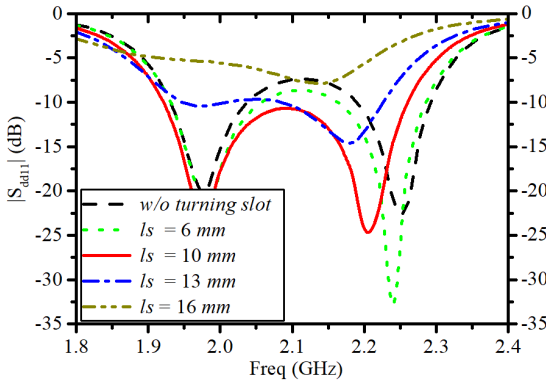


**FIGURE 9.** The differential-mode reflection coefficient of the complementary MPA.

There is a detailed design in which a tiny slot is added on the top layer of the QMSIW cavity, which is considered for turning the impedance match. In Fig. 9, the effect of the length of the turning slot is demonstrated. The wide frequency band divides into two isolated bands without the turning slot. Introducing a turning slot with increasing length has no essential effect on the lower resonant frequency, while the higher resonant point is sensitive to the variation. The slot can make the surface current path of the QMSIW cavity roundabout, which can cause the resonant frequency of the QMSIW cavity to shift to the low end, like the trend of the higher resonant point in Fig. 9. While a long slot will damage the coupling mechanism between the QMSIW cavity and the MPA, as shown in Fig. 9, the port performance will dramatically degrade when the turning slot is too long.

Since the loaded monopole can essentially change the radiation characteristics of the MPA, the monopole is worth focusing on. First, the triangular monopole is a typical wideband radiator that can simplify the optimization work and make it easier to adjust the two components of the complementary source with similar radiation amplitudes. Second, the length of the monopole is the key parameter for the FBR, as shown in Fig. 10, and changing the length of the monopole changes the maximum value of the FBR and its corresponding frequency. The length of the monopole can affect the radiation intensity of the monopole, which is the magnitude of the 8-shaped pattern in Fig. 5(b). Theoretically, a suitable monopole radiation intensity based on a decent monopole length can realize perfect backward radiation suppression. The monopoles also have an effect on the port performance, mainly at higher frequency resonance points, while the port characteristics are generally a good match. Hence, the loaded monopoles mainly influence the radiation performance without having an essential effect on the port performance of the MPA.

## IV. EXPERIMENT AND DISCUSSION

To verify the previous analysis and the effectiveness of the improved HMSIW/QMSIW-cavity feeding mechanism, as shown in Fig. 11, a differential dual-polarized prototype based on Fig. 8 is fabricated and tested. The whole model

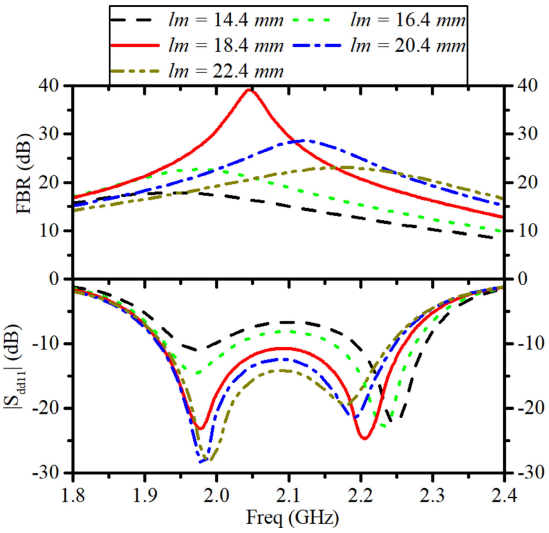


**FIGURE 10.** The differential-mode reflection coefficient of the complementary MPA.

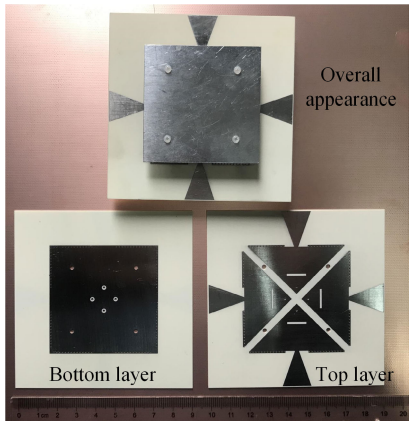


**FIGURE 11.** The differential-mode reflection coefficient of complementary MPA.

is constructed with an aluminum patch as the radiator and a substrate designed on the QMSIW cavities and loaded monopoles.

### A. PORT PERFORMANCE

The measured reflection coefficient curves and differential port-to-port isolation are compared with simulated ones in Fig. 12 and Fig. 13, respectively. The simulated $|S_{dd11}|$ and $|S_{dd22}|$ are perfectly coincident, so they are represented by a curve. The good agreement between the measured $|S_{dd11}|$ and $|S_{dd22}|$ also verifies this feature. Based on the standard of $|S_{dd11}|/|S_{dd22}| < -10\ dB$, the measured impedance bandwidth (15.4%, 1.91 GHz - 2.23 GHz) is slightly narrower than the simulated results (16.3%, 1.92 GHz - 2.26 GHz). The main difference is that the higher resonant frequency shift to the low end. Based on the previous analysis (Section III, B), the higher resonant point is mainly determined by the QMSIW cavities, so the measured result error can be attributed to the potential thickness and dielectric constant instability of the dielectric substrate. There is an

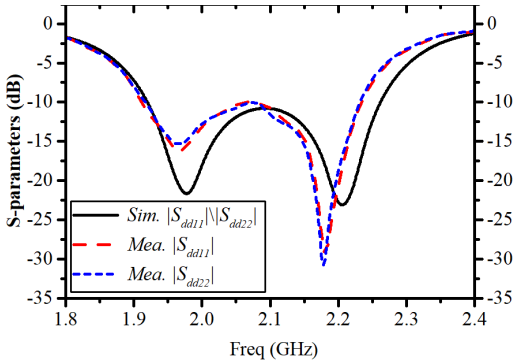


**FIGURE 12.** The differential-mode reflection coefficient of the complementary MPA.

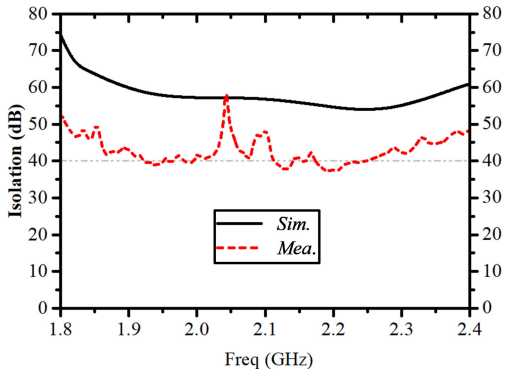


**FIGURE 13.** The differential port-to-port isolation of the complementary MPA.

obvious gap between the simulated differential port-to-port isolation and the measured results caused by fabrication error. At the same time, the test error also makes the measured isolation curve not as smooth as the simulation one.

The reflection coefficients and differential isolations are defined in [37]. $|S_{dd11}|$, $|S_{dd22}|$, $|S_{dd12}|$ and $|S_{dd21}|$ can be transformed from the single-end S-parameters of the four-port network using the following formulas.

$$S_{dd11} = (S_{1+1+} - S_{1+1-} - S_{1-1+} + S_{1-1-})/2 \quad (1)$$
$$S_{dd11} = (S_{2+2+} - S_{2+2-} - S_{2-2+} + S_{2-2-})/2 \quad (2)$$
$$S_{dd21} = (S_{1-1+} - S_{2-1+} - S_{1-2+} + S_{2-1-})/2 \quad (3)$$
$$S_{dd12} = (S_{1+2+} - S_{1+2-} - S_{2+1-} + S_{1-2-})/2 \quad (4)$$

### B. RADIATION PERFORMANCE

Comparing the measured gain and simulated gain in Fig. 14 shows good agreement between the measured results and simulated results. The stable antenna gain in the operating band is approximately 7.5 dBi, and the fluctuation in the antenna gain is lower than 1 dB. Compared to the simulated results, the measured 1-dB gain bandwidth is somewhat narrow with the same trend as the reflection coefficient curves. In addition, the antenna has an excellent antenna efficiency over 0.95 in the operating band (Fig. 14).

The FBR performance is the main discussion point of this paper. The simulated results show a greater than 18 dB FBR over the whole band with a maximum value of 38 dB at

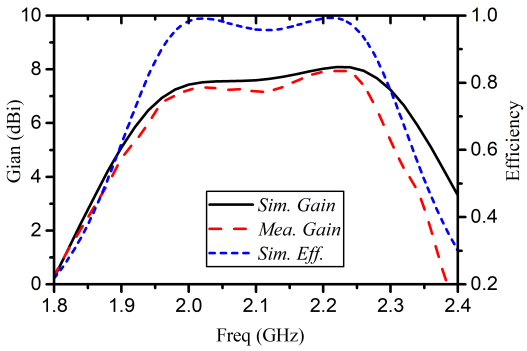


**FIGURE 14.** The gain and antenna efficiency of the complementary MPA.

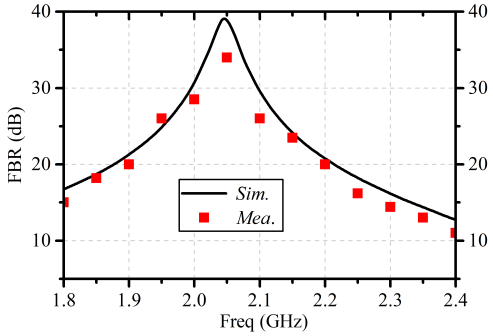


**FIGURE 15.** The FBR of the wideband complementary MPA.

2.04 GHz, while this parameter is greater than 18 dB in the measured band with a maximum value of 34 dB at 2.05 GHz. In general, the simulation results and measured results exhibit the same trends and acceptable agreement.

The normalized radiation patterns in the E-plane/H-plane at 1.94 GHz, 2.06 GHz and 2.2 GHz of the fabricated prototype when differential port_1 is excited are compared in Fig. 16. Similar radiation patterns can be observed when differential port_2 is driven, but these results are not shown here for simplicity. Great agreement between the measured copolarization and the simulated results can be found. The measured cross-polarization is approximately 20 dB, while the simulated cross-polarization is not described because it is less than the range shown in Fig. 16. The large gap between the simulated cross-polarization and experiment is caused by assembly errors and the limited dynamic range of the test system. The excellent back radiation suppression performance can also be confirmed by the measured radiation pattern. In particular, Fig. 16 (b) shows a clear and precise back-radiation zero.

### C. DISCUSSION

Interestingly, the radiation pattern of the complementary antennas should have been heart-type, as shown in Fig. 5 (b), while both the simulated and measured results, as shown in Fig. 16, show that this is the case only for the radiation pattern in the H-plane and that the radiation pattern in the E-plane is clearly different. There are two radiation quasizeros at $\theta = -90°$ and $\theta = 90°$. The reason can be traced back to the radiation source model. In the E-plane, the radiation sources can be considered to be a two-element

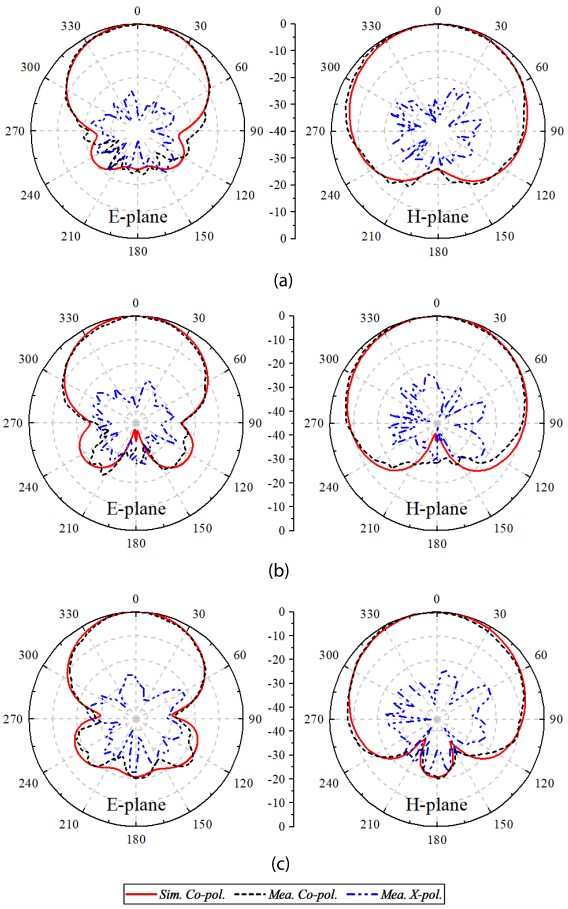


**FIGURE 16.** The radiation patterns of the complementary MPA at (a) 1.94 GHz, (b) 2.06 GHz and (c) 2.2 GHz.

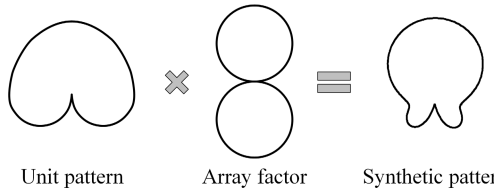


**FIGURE 17.** The E-plane radiation pattern synthesis mechanism of the complementary HMSIW/QMSIW-fed MPA.

array with complementary units, and the distance between the two complementary elements is approximately the width of the radiation patch, which is approximately $0.4\lambda_0$ in these proposed MPAs. Therefore, the theoretical radiation pattern should be the typical complementary source radiation pattern synthesized with an equivalent amplitude and phase excitation binary array factor with a unit space of $0.4\lambda_0$, as illustrated in Fig. 17. Obviously, acceptable agreement can be found in a comparison of the synthetic theoretical radiation pattern in Fig. 17 and the simulated/measured radiation pattern in Fig. 16 (b).

Finally, a comparison between this prototype and previously reported differential wideband MPAs is listed in Table 1. Obviously, this work developed a decent wideband performance. More importantly, this prototype achieved an excellent FBR performance based on a compact size.

**TABLE 1.** Performance comparison between different differential-fed wideband MPAs.

| Ref. | [14] | [15] | [16] | [24] | This work |
|---|---|---|---|---|---|
| Feed type | diff. | diff. | diff. | diff. | diff. |
| Polarization | line | line | dual. | line | dual. |
| size($\times\lambda_0{}^*$) | $1.27\times 1.27$ | NA. | $1.89\times 1.89$ | $1.23\times 1.14$ | $0.66\times 0.66$ |
| Profile ($\times\lambda_0{}^*$) | 0.039 | 0.037 | 0.024 | 0.013 | 0.04 |
| Center-frequency | 1.9 | 3.5 | 1.72 | 2.45 | 2.09 |
| Bandwidth | 10% | 11.4% | 8% | 4% | 15.4% |
| Gain(dBi) | 10 | 9 | 7 | 5 | 7 |
| FBR(dB) | 10 | 20 | 12 | 20 | 34 |
| XPD (dB) | 23 | 25 | 22.6 | NA. | 20 |

## V. CONCLUSION

A new wideband MPA is proposed in this paper. The impedance bandwidth of the proposed antenna is enhanced by the HMSIW/QMSIW cavity as the feeding structure. Additionally, the concept of complementary radiation sources is applied to suppress the back radiation of the MPAs. The orthogonal complementary sources are constructed by the equivalent radiation magnetic currents of the MPAs and a loaded monopole fed by the HMSIW/QMSIW cavity. To highlight the effect of the introduction of complementary sources, a differential feeding scheme is adopted for symmetrical radiation performance. Both the line-polarized model differentially fed by the improved HMSIW cavity and the dual-polarized model differentially fed by the improved QMSIW cavity are analyzed, and the dual-polarized case is fabricated and tested. The measured results show an enhanced bandwidth of 15.4% with a high differential port-to-port isolation of over 38 dB and a maximum FBR of 34 dB with an average gain of 7.5 dBi in the operating band.

## REFERENCES

[1] R. Garg, P. Bhartia, I. J. Bahl, and A. Ittipiboon, *Microstrip Antenna Design Handbook*. Norwood, MA, USA: Artech House, 2001.

[2] J. Howell, "Microstrip antennas," *IEEE Trans. Antennas Propag.*, vol. AP-23, no. 1, pp. 90–93, Jan. 1975.

[3] A. Derneryd, "Linearly polarized microstrip antennas," *IEEE Trans. Antennas Propag.*, vol. AP-24, no. 6, pp. 846–851, Nov. 1976.

[4] Y. Cao, Y. Cai, W. Cao, B. Xi, Z. Qian, T. Wu, and L. Zhu, "Broadband and high-gain microstrip patch antenna loaded with parasitic mushroom-type structure," *IEEE Antennas Wireless Propag. Lett.*, vol. 18, no. 7, pp. 1405–1409, Jul. 2019.

[5] P. B. Parmar, B. J. Makwana, and M. A. Jajal, "Bandwidth enhancement of microstrip patch antenna using parasitic patch configuration," in *Proc. Int. Conf. Commun. Syst. Netw. Technol.*, May 2012, pp. 53–57.

[6] W. Cao and W. Hong, "Bandwidth and gain enhancement for single-fed compact microstrip antenna by loading with parasitical patches," in *Proc. IEEE Int. Conf. Microw. Millim. Wave Technol. (ICMMT)*, vol. 2, Jun. 2016, pp. 650–652.

[7] L. Guo and M.-C. Tang, "A low-profile dual-polarized patch antenna with bandwidth enhanced by stacked parasitic elements," in *Proc. Int. Conf. Microw. Millim. Wave Technol. (ICMMT)*, May 2018, pp. 1–3.

[8] K. M. Luk, C. L. Mak, Y. L. Chow, and K. F. Lee, "Broadband microstrip patch antenna," *Electron. Lett.*, vol. 34, no. 15, pp. 1442–1443, Jul. 1998.

[9] K. M. Mak, H. W. Lai, and K. M. Luk, "A 5G wideband patch antenna with antisymmetric L-shaped probe feeds," *IEEE Trans. Antennas Propag.*, vol. 66, no. 2, pp. 957–961, Feb. 2018.

[10] H.-W. Lai and K.-M. Luk, "Dual polarized patch antenna fed by meandering probes," *IEEE Trans. Antennas Propag.*, vol. 55, no. 9, pp. 2625–2627, Sep. 2007.
[11] H.-W. Lai and K.-M. Luk, "Design and study of wide-band patch antenna fed by meandering probe," *IEEE Trans. Antennas Propag.*, vol. 54, no. 2, pp. 564–571, Feb. 2006.
[12] D. M. Pozar, "Microstrip antenna aperture-coupled to a microstripline," *Electron. Lett.*, vol. 21, no. 1, pp. 49–50, Jan. 1985.
[13] F. Croq and A. Papiernik, "Large bandwidth aperture-coupled microstrip antenna," *Electron. Lett.*, vol. 26, no. 16, pp. 1293–1294, Aug. 1990.
[14] N.-W. Liu, L. Zhu, W.-W. Choi, and X. Zhang, "A low-profile differential-fed patch antenna with bandwidth enhancement and sidelobe reduction under operation of $TM_{10}$ and $TM_{12}$ modes," *IEEE Trans. Antennas Propag.*, vol. 66, no. 9, pp. 4854–4859, Sep. 2018.
[15] Q. Liu, L. Zhu, J. Wang, and W. Wu, "Wideband low-profile differential-fed patch antennas with an embedded SIW cavity under dual-mode resonance," *IEEE Trans. Antennas Propag.*, vol. 67, no. 6, pp. 4235–4240, Jun. 2019.
[16] N.-W. Liu, L. Zhu, X. Zhang, and W.-W. Choi, "A wideband differential-fed dual-polarized microstrip antenna under radiation of dual improved odd-order resonant modes," *IEEE Access*, vol. 5, pp. 23672–23680, 2017.
[17] N.-W. Liu, L. Zhu, W.-W. Choi, and J.-D. Zhang, "A low-profile differentially fed microstrip patch antenna with broad impedance bandwidth under triple-mode resonance," *IEEE Antennas Wireless Propag. Lett.*, vol. 17, no. 8, pp. 1478–1482, Aug. 2018.
[18] N. Liu, L. Zhu, and W. Choi, "A differential-fed microstrip patch antenna with bandwidth enhancement under operation of $TM_{10}$ and $TM_{30}$ modes," *IEEE Trans. Antennas Propag.*, vol. 65, no. 4, pp. 1607–1614, Apr. 2017.
[19] M. T. Islam, N. Misran, M. N. Shakib, and B. Yatim, "Low cross-polarization broadband microstrip patch antenna," in *Proc. 6th Nat. Conf. Telecommun. Technol. 2nd Malaysia Conf. Photon.*, Aug. 2008, pp. 144–147.
[20] M. Pour, M. Henley, A. Young, and Z. Iqbal, "Cross-polarization reduction in offset reflector antennas with dual-mode microstrip primary feeds," *IEEE Antennas Wireless Propag. Lett.*, vol. 18, no. 5, pp. 926–930, May 2019.
[21] R. Dehbashi, Z. Atlasbaf, and K. Forooraghi, "New compact size microstrip antennas with harmonic rejection," *IEEE Antennas Wireless Propag. Lett.*, vol. 5, pp. 395–398, 2006.
[22] Y. Xu, S. Gong, and T. Hong, "Circularly polarized slot microstrip antenna for harmonic suppression," *IEEE Antennas Wireless Propag. Lett.*, vol. 12, pp. 472–475, 2013.
[23] Y. Zang, H. Zhai, L. Xi, and L. Li, "A compact microstrip antenna with enhanced bandwidth and ultra-wideband harmonic suppression," *IEEE Trans. Antennas Propag.*, vol. 67, no. 3, pp. 1969–1974, Mar. 2019.
[24] D. Wang, X.-C. Wei, J.-B. Zhang, Y.-F. Shu, and D.-C. Yang, "Back lobe reduction of patch antenna by using high-impedance surface (invited)," in *Proc. IET Int. Radar Conf.*, Oct. 2015, pp. 1–4.
[25] H. Alias, M. T. Ali, S. S. N. Ramli, M. A. Sulaiman, and S. Kayat, "A back lobe reduction of aperture coupled microstrip antenna using DGS," in *Proc. 10th Int. Conf. Electr. Eng./Electron., Comput., Telecommun. Inf. Technol.*, May 2013, pp. 1–5.
[26] C. Jin, R. Li, A. Alphones, and X. Bao, "Quarter-mode substrate integrated waveguide and its application to antennas design," *IEEE Trans. Antennas Propag.*, vol. 61, no. 6, pp. 2921–2928, Jun. 2013.
[27] T. Deckmyn, S. Agneessens, A. C. F. Reniers, A. B. Smolders, M. Cauwe, D. V. Ginste, and H. Rogier, "A novel 60 GHz wideband coupled half-mode/quarter-mode substrate integrated waveguide antenna," *IEEE Trans. Antennas Propag.*, vol. 65, no. 12, pp. 6915–6926, Dec. 2017.
[28] A. Chlavin, "A new antenna feed having equal E -and H-plane patterns," *Trans. IRE Prof. Group Antennas Propag.*, vol. 2, no. 3, pp. 113–119, Jul. 1954.
[29] D.-H. Kwon, "On the radiation $Q$ and the gain of crossed electric and magnetic dipole moments," *IEEE Trans. Antennas Propag.*, vol. 53, no. 5, pp. 1681–1687, May 2005.
[30] K.-M. Luk and B. Wu, "The magnetoelectric dipole—A wideband antenna for base stations in mobile communications," *Proc. IEEE*, vol. 100, no. 7, pp. 2297–2307, Jul. 2012.
[31] M.-C. Tang, B. Zhou, and R. W. Ziolkowski, "Low-profile, electrically small, Huygens source antenna with pattern-reconfigurability that covers the entire azimuthal plane," *IEEE Trans. Antennas Propag.*, vol. 65, no. 3, pp. 1063–1072, Mar. 2017.
[32] M.-C. Tang, T. Shi, and R. W. Ziolkowski, "A study of 28 GHz, planar, multilayered, electrically small, broadside radiating, Huygens source antennas," *IEEE Trans. Antennas Propag.*, vol. 65, no. 12, pp. 6345–6354, Dec. 2017.
[33] K. Sun, Y. Zhao, D. Yang, and J. Pan, "A single-layer differential substrate-integrated slot antenna with common-mode rejection," *IEEE Antennas Wireless Propag. Lett.*, vol. 18, no. 2, pp. 392–396, Feb. 2019.
[34] T. Brauner, R. Vogt, and W. Bachtold, "A differential active patch antenna element for array applications," *IEEE Microw. Wireless Compon. Lett.*, vol. 13, no. 4, pp. 161–163, Apr. 2003.
[35] E. Lee, K. M. Chan, P. Gardner, and T. E. Dodgson, "Active integrated antenna design using a contact-less, proximity coupled, differentially fed technique," *IEEE Trans. Antennas Propag.*, vol. 55, no. 2, pp. 267–276, Feb. 2007.
[36] Z.-Y. Zhang and K.-L. Wu, "Double torsion coil feeding structure for patch antennas," *IEEE Trans. Antennas Propag.*, vol. 67, no. 6, pp. 3688–3694, Jun. 2019.
[37] W. Eisenstadt, R. Stengel, and B. Thompson, *Microwave Differential Circuit Design Using Mixed Mode S-Parameters*. Norwood, MA, USA: Artech House, 2006.

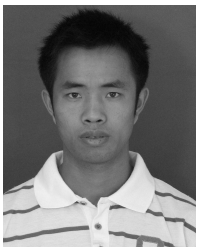

**LIPING YUAN** received the B.E. degree from the Chengdu University of Information Technology, in 2011, and the M.E. degree from the School of Electronic Engineering, University of Electronic Science and Technology of China, in 2014. He is currently working with the University of Electronic Science and Technology. His research interests include microwave circuits and microstrip antenna technology.

**KAI SUN** received the B.E. degree from the School of Electronic Engineering, University of Electronic Science and Technology of China (UESTC), in 2016, where he is currently pursuing the M.S. degree. His research interests include antenna design and theory and multifeed antennas.

**SIHAO LIU** received the B.E. and M.E. degrees from the School of Electronic Engineering, University of Electronic Science and Technology of China (UESTC), in 2013 and 2016, respectively, where he is currently pursuing the Ph.D. degree. His research interests include metasurface antenna, antenna design using CMA, UWB antennas, microwave power transmission, and MIMO technology.

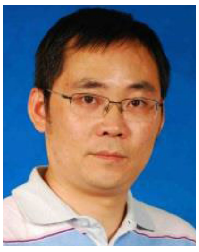

**BO CHEN** (Member, IEEE) received the B.S. degree from the University of Electronic Science and Technology of China (UESTC). He is currently an Associate Professor with UESTC. His research interests include microwave and millimeter wave measurement, antenna design, and electromagnetic compatibility and protection.

**DEQIANG YANG** (Member, IEEE) received the B.E., M.E., and D.E. degrees from the School of Electronic Engineering, University of Electronic Science and Technology of China (UESTC), in 1992, 2006, and 2012, respectively. From 2012 to 2016, he was a Senior Engineer with UESTC. His research interests include UWB indoor localization technology, antenna measurement, and antenna theory.